Nano Research Energy

ISSN 2791-0091 (print); 2790-8119 (online)
https://doi.org/10.26599/NRE.2025.9120211

Research Article

Achieving durable alkaline seawater oxidation over NiFe layered double hydroxide via sulfur doping

Hua Chen[1,2], Mingyu Liu[3], Zhenju Jiang[4], Shengjun Sun[3], Imran Shakir[5], Shuai Hou[6] (✉), and Xuping Sun[1,3] (✉)

[1] *Chengdu Investment Promotion Bureau, Chengdu 610041, China*
[2] *Center for High Altitude Medicine, West China Hospital, Sichuan University, Chengdu 610041, China*
[3] *College of Chemistry, Chemical Engineering and Materials Science, Shandong Normal University, Jinan 250014, China*
[4] *College of Science, Xihua University, Chengdu 610039, China*
[5] *Department of Physics, Faculty of Science, Islamic University of Madinah, Madinah 42351, Saudi Arabia*
[6] *Key Laboratory of Architectural Cold Climate Energy Management, School of Materials Science and Engineering, Jilin Jianzhu University, Changchun 130118, China*

Received: 30 October 2025 / **Revised:** 20 November 2025 / **Accepted:** 26 November 2025 / **Published date:** 17 December 2025

ABSTRACT

Alkaline seawater electrolysis is promising for large-scale production of green hydrogen but the chlorine evolution reaction (CER) causes severe anode's corrosion under high current densities. This work described the use of a sulfur-doped NiFe layered double hydroxide nanoarray on Ni foam (S-NiFe LDH/NF) synthesized through a two-step hydrothermal process as a durable catalyst for alkaline seawater oxidation. In 1 M KOH + seawater, the S-NiFe LDH/NF anode needs a low overpotential of 345 mV to afford a current density of 1000 mA·cm^{-2} and operates stably over 800 h. Sulfate species generated on the catalyst surface, which is evidenced by *in situ* Raman spectroscopy analysis, electrostatically repel Cl^- and thus inhibits the CER. Furthermore, the two-electrode system using S-NiFe LDH/NF and Pt/C/NF as the anode and cathode, respectively, requires a cell voltage of 1.90 V to achieve a current density of 100 mA·cm^{-2} and maintains stable operation for 1000 h at 500 mA·cm^{-2} in alkaline seawater.

KEYWORDS

seawater electrolysis, oxygen evolution reaction, NiFe LDH, sulfur doping, anti-chlorine corrosion

1 Introduction

As a zero-emission clean energy vector alternative to traditional fossil fuels, hydrogen (H_2) plays a crucial role in realizing the global carbon neutrality target [1]. H_2 also offers strong antioxidation capacities with important implications for health and diseases and recent years have witnessed its intensive applications as an effective therapeutic antioxidant to scavenge harmful oxygen radicals [2, 3]. Currently, green H_2 production mainly relies on water electrolysis technique driven by renewable energy [4–6]; however, a tiny fraction, only 2.5%, of the Earth's water is fresh and available for use [7, 8], raising concerns about global freshwater scarcity and widespread adoption of water-splitting technology. Seawater electrolysis has attracted considerable recent research interest but is challenged by precipitate coverage on the cathode, meanwhile on the anode, the competitive chlorine evolution reaction (CER) generates corrosive chlorine compounds (ClO^-, HClO) instead of the preferred oxygen evolution reaction (OER) in view of the presence of diverse cations and anions in seawater [9–27]. While the acidic environment can circumvent certain issues inherent to alkaline systems [28], it faces significant challenges in addressing the severe competition from the CER at the anode. In contrast, the alkaline system provides more favorable thermodynamic conditions for suppressing these competitive anode reactions [29]. Furthermore, in alkaline seawater, the cathodic precipitation of calcium and magnesium hydroxides precipitation issue can be avoided, but it is still in great need to prolong the anode's lifespan for durable alkaline seawater oxidation (ASO) at industrial-level current densities (*j*).

Layered double hydroxides (LDHs) have explored as extensively reported OER catalysts [30–33]. Great recent efforts have also been devoted to exploiting their uses as ASO catalysts with high OER activity [16–21, 34–42]. Creating an anionic layer holds great promise as an effective strategy to enhance the anode's anti-chlorine corrosion performance due to that the electrostatic repulsion between such anions and Cl^- in seawater avoids the direct contact of Cl^- with the catalyst. Interestingly, the positively charged host layers for LDHs facilitate the intercalation or surface adsorption of charge-compensating anions [43, 44], thereby advantaging the easy introduction of Cl^--repelling block layer.

Address correspondence to Shuai Hou, housua@163.com; Xuping Sun, xpsun@uestc.edu.cn

Indeed, various anions have been successfully adopted in this scenario [17, 18, 20, 21, 35–37, 41, 42, 45]. SO_4^{2-} also performs well for such an application [38, 39]. Kuang et al. constructed a catalyst by growing NiFe LDH on a NiS_x-coated Ni foam (NiFe/NiS_x-Ni), and the *in situ*-generated polyatomic sulfate ions diffused to the NiFe catalyst, forming an anion-rich passivating layer for chloride repel [38]. Chen et al. achieved durable alkaline seawater oxidation on NiFe LDH via Ba doping and SO_4^{2-} in the electrolyte was adsorbed on LDH via the chemical fixation by Ba^{2+} and the polarization effect [39].

Here, we report a sulfur-doped NiFe LDH nanoarray on Ni foam (S-NiFe LDH/NF), fabricated by a two-step solvothermal process, for application in durable alkaline seawater oxidation (ASO). This S-NiFe LDH/NF acquires an industrial-level *j* of 1000 mA·cm^{-2} at a remarkably low overpotential of merely 345 mV, and showcases exceptional durability with 800 h. *In situ* Raman spectroscopy analysis demonstrates the dual role of sulfur doping in facilitating the conversion of active sites and the fabrication of SO_4^{2-} on NiFe LDH surface during ASO. The observation of minimal signals of active chlorine species for S-NiFe LDH/NF further shows its remarkable Cl^- corrosion resistance. The two-electrode electrolyzer (S-NiFe LDH/NF||Pt/C/NF) demonstrated remarkable operational stability with continuous 1000 h operation at 500 mA·cm^{-2} in alkaline seawater.

2 Results and discussion

The fabrication of S-NiFe LDH/NF is schematically depicted in Fig. 1(a). The X-ray diffraction (XRD) patterns (Fig. 1(b)) show that all diffraction peaks match well with those of reference NiFe LDH (PDF#40-0215) and the NF substrate (PDF#04-0850). Scanning electron microscopy (SEM) images reveal that the morphology remains largely unchanged after sulfur doping, with both samples exhibiting a uniform nanosheet structure (Fig. 1(c), Figs. S1 and S2 in the Electronic Supplementary Material (ESM)). The nanosheet morphology was further revealed by transmission electron microscopy (TEM) (Fig. 1(d)). The crystal structure was further confirmed by HRTEM (Fig. 1(e)), which showed a lattice spacing of 0.250 nm, attributable to the (012) plane of NiFe LDH. Additionally, the elemental composition and distribution character of S-NiFe LDH, comprising Ni, Fe, C, O, and S, was revealed by the corresponding elemental mapping (Fig. 1(f)). The surface chemical state of the catalyst was probed by X-ray photoelectron spectroscopy (XPS) (Fig. S3 in the ESM). The Ni 2p XPS spectrum identified the presence of doublet peaks for Ni^{2+} and Ni^{3+} species, as evidenced by the Ni 2p signals at 856.1/873.8 eV and 857.9/876.1 eV, respectively, along with their satellite peaks (862.5, 880.2 eV) in Fig. S4(a) in the ESM [46]. In the Fe 2p region (Fig. S4(b) in the ESM), characteristic signals of Fe^{2+} (706.7/719.0 eV) and Fe^{3+} (711.4/725.7 eV) are observed, further confirming the mixed-valence state of the catalyst [41, 47]. Conversely, the O 1s spectrum in Fig. S4(c) in the ESM presents three distinct contributions, corresponding to lattice oxygen (529.5 eV), metal hydroxides (531.2 eV), and adsorbed water (532.0 eV) [48]. XPS analysis of the S 2p region (Fig. S4(d) in the ESM) confirms the presence of M–S bonds (162.3, 163.6 eV) and a S–O species (168.0 eV) [49, 50]. Concurrently, the negative shifts in the Ni 2p and Fe 2p signal represent a signature of the electron-rich environment induced by the incorporated sulfur.

The catalytic performance was investigated via linear sweep voltammetry (LSV) in alkaline seawater (1 M KOH + seawater). Details of the seawater used in the experiments can be found in Table S1 in the ESM. To achieve optimal performance, the effect of the amount of thiourea was investigated. As presented in Fig. S5 in the ESM, the best performance was obtained when 0.2 g of S

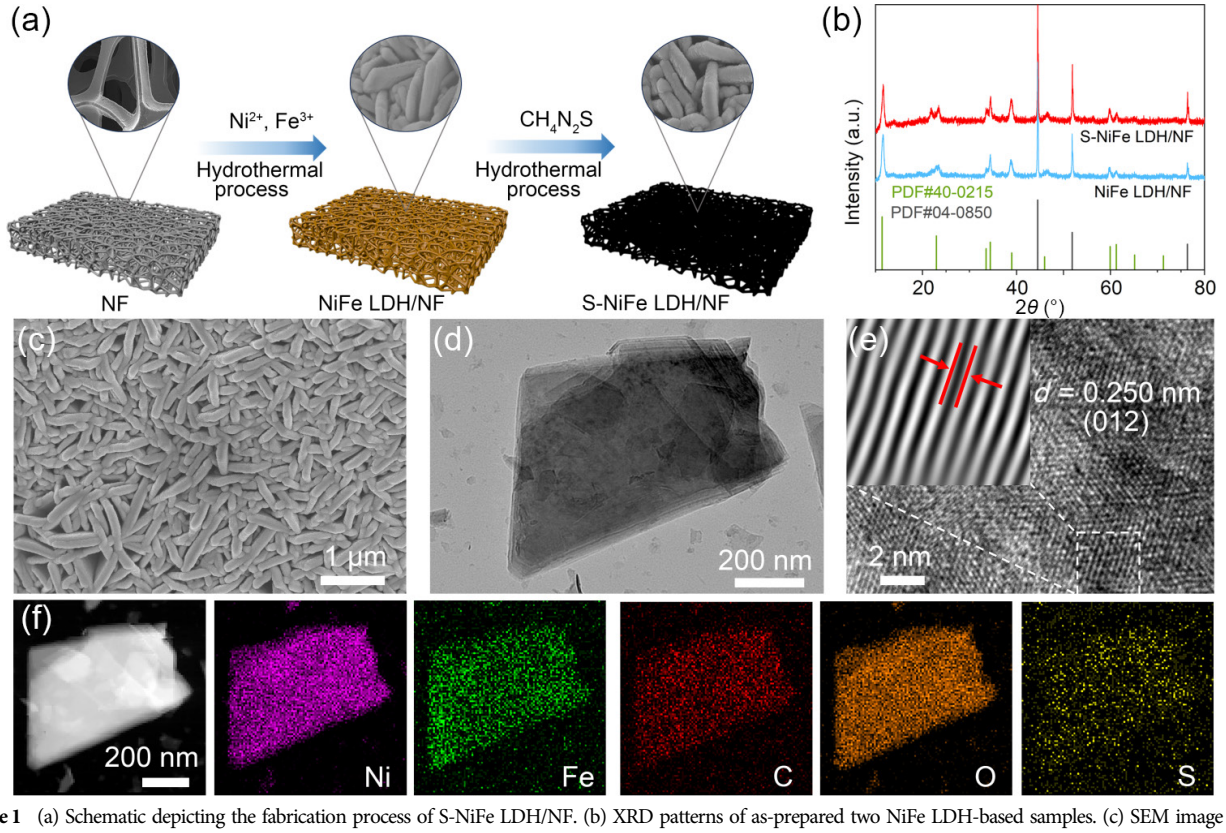

Figure 1 (a) Schematic depicting the fabrication process of S-NiFe LDH/NF. (b) XRD patterns of as-prepared two NiFe LDH-based samples. (c) SEM image of S-NiFe LDH/NF. (d)–(f) TEM, HRTEM, and elemental mapping of S-NiFe LDH.

was used. The S-NiFe LDH/NF anode demonstrates outstanding electrocatalytic activity, requiring significantly lower overpotentials of only 307 and 345 mV to reach 500 and 1000 mA·cm^{-2}, respectively, substantially outperforming that of both NiFe LDH/NF (354 mV) and RuO_2/NF (550 mV) at the same j (Figs. 2(a) and 2(b)) (LSV curves without iR compensation are shown in Fig. S6 in the ESM). Notably, a Tafel slope of 31.15 mV·dec^{-1} indicates that the catalyst possesses superior OER kinetics (Fig. S7 in the ESM). The turnover frequency (TOF) was calculated to be 2.46 s^{-1} for S-NiFe LDH/NF at an η of 0.35 V (Fig. 2(a) inset, Figs. S8 and S9 in the ESM), superior to the 1.95 s^{-1} recorded for NiFe LDH/NF and RuO_2/NF (1.07 s^{-1}), confirming its greater catalytic efficiency. Electrochemical impedance spectroscopy (EIS) analysis presents S-NiFe LDH/NF possesses a significantly lower charge transfer resistance (R_{ct} = 6.50 Ω) relative to undoped sample (R_{ct} = 8.33 Ω) at the same potential (Fig. S10 and Table S2 in the ESM). Additionally, potential-dependent EIS measurements are conducted, showing that a gradual reduction in R_{ct} was observed with increasing potential with the potential increasing from 1.424 to 1.524 V (Fig. S11 in the ESM), as evidenced by the shrinking semicircle diameter in the Nyquist plot, further presenting its superior charge transfer efficiency. Meanwhile, sulfur doping markedly enhanced the reaction kinetics, as confirmed by the substantial reduction in activation energy to 26.97 kJ·mol^{-1} for S-NiFe LDH/NF from 34.72 kJ·mol^{-1} for the undoped analogue, underscoring its role in lowering the energetic barrier (Fig. 2(c) and Fig. S12 in the ESM). *In situ* Raman spectroscopy (Figs. 2(d) and 2(e)) reveals two vibrational signatures at 453 and 529 cm^{-1} under low potential, which are characteristic of the Ni^{II}–OH and Ni^{II}–O stretching modes, respectively [51, 52]. Noted that a concomitant shift of these peaks to 475 and 553 cm^{-1} is observed at higher potentials, signifying the transformation to NiOOH phase [20, 53]. Notably, the characteristic peak of the catalyst shifted at a lower potential. This transition confirms that sulfur doping accelerates the catalyst's surface reconstruction and promotes the formation of highly active Ni^{3+} species [54]. Furthermore, Fourier transform alternating current voltammetry (FTacV) measurements were additionally employed to probe the surface redox behavior. As shown in Fig. 2(f), both catalysts show a characteristic current response in Region 1, associated with the oxidation of nickel species from low oxidation state (Ni^{2+}) to high oxidation state (Ni^{3+}). A further structural evolution in Region 2 yields the active NiOOH sites. The catalyst exhibits a higher current response in this region, indicating that its structure undergoes reconstruction more rapidly. This also accounts for the high OER activity observed in Region 3 for the catalyst electrode. The integrated areas of profiles from diverse regions, combined with the LSV results, corroborate the above findings (Figs. S13 and S14 in the ESM).

At an industrial-level j of 1000 mA·cm^{-2}, the electrochemical durability of S-NiFe LDH/NF catalyst was evaluated, which exhibited significantly enhanced operational stability performance for over 800 hours, demonstrating markedly superior stability compared to NiFe LDH/NF (only 180 hours) (Fig. 3(a)). The S-NiFe LDH/NF electrode demonstrates stability competitive with the previously reported catalysts, as evidenced by the comparative result summarized in Fig. 3(b) and Table S3 in the ESM. After conducting the stability test, we examined its morphology and chemical composition. As shown in Fig. S15 in the ESM, only minor changes occurred in the morphology of the catalyst after the stability test. As revealed by the XPS analysis of Ni 2p and Fe 2p regions, Ni and Fe are in a high oxidation state following the stability test (Fig. S16 in the ESM). Following the prolonged potentiostatic test, inductively coupled plasma optical emission spectrometry (ICP-OES) analysis revealed that the leaching amounts of Ni and Fe from the S-NiFe LDH/NF were significantly lower than those from the unmodified NiFe LDH/NF, demonstrating its superior structural stability (Table S4 in the ESM). Additionally, the catalyst exhibits robust stability, demonstrating negligible activity loss after 5000 cycles, which is corroborated by the superimposable LSV profiles (Fig. S17 in the ESM). To determine the residual active chlorine level, the post-electrolysis electrolyte was explored with the help of the N, N-

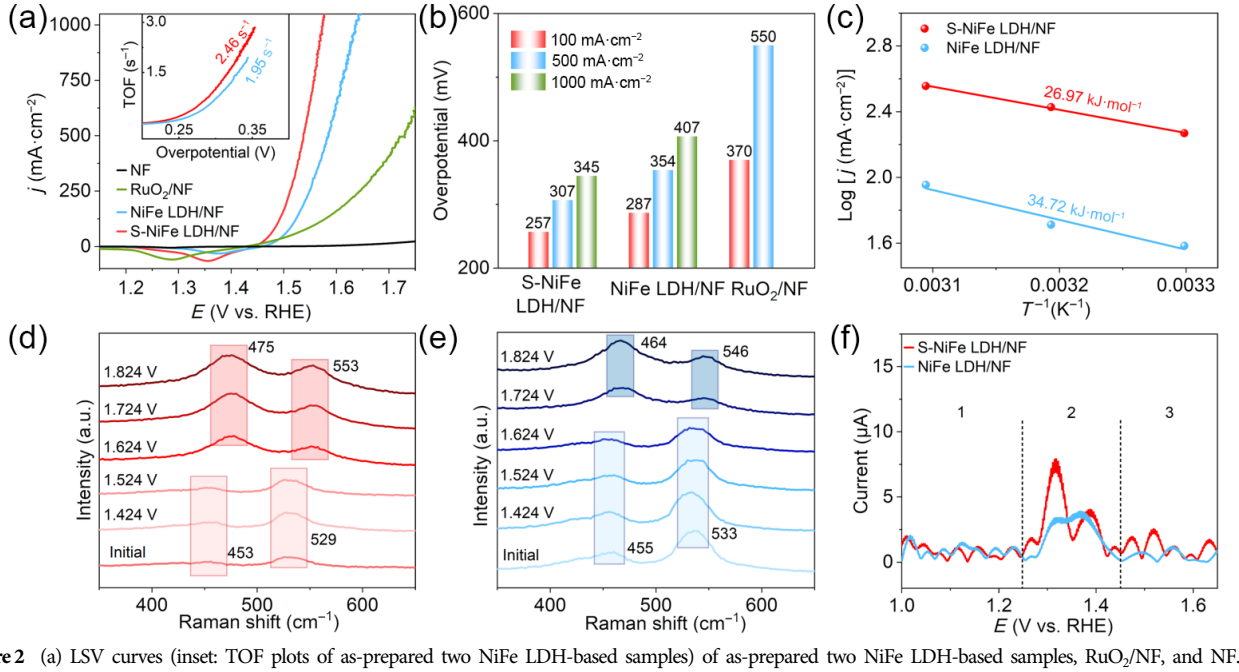

Figure 2 (a) LSV curves (inset: TOF plots of as-prepared two NiFe LDH-based samples) of as-prepared two NiFe LDH-based samples, RuO_2/NF, and NF. (b) Comparison of overpotentials of S-NiFe LDH/NF, NiFe LDH/NF, and RuO_2/NF in 1 M KOH + seawater. (c) Activation energy plots for as-prepared two NiFe LDH-based samples. *In situ* electrochemical Raman spectra of (d) S-NiFe LDH/NF and (e) NiFe LDH/NF. (f) FTacV curves for as-prepared two NiFe LDH-based samples.

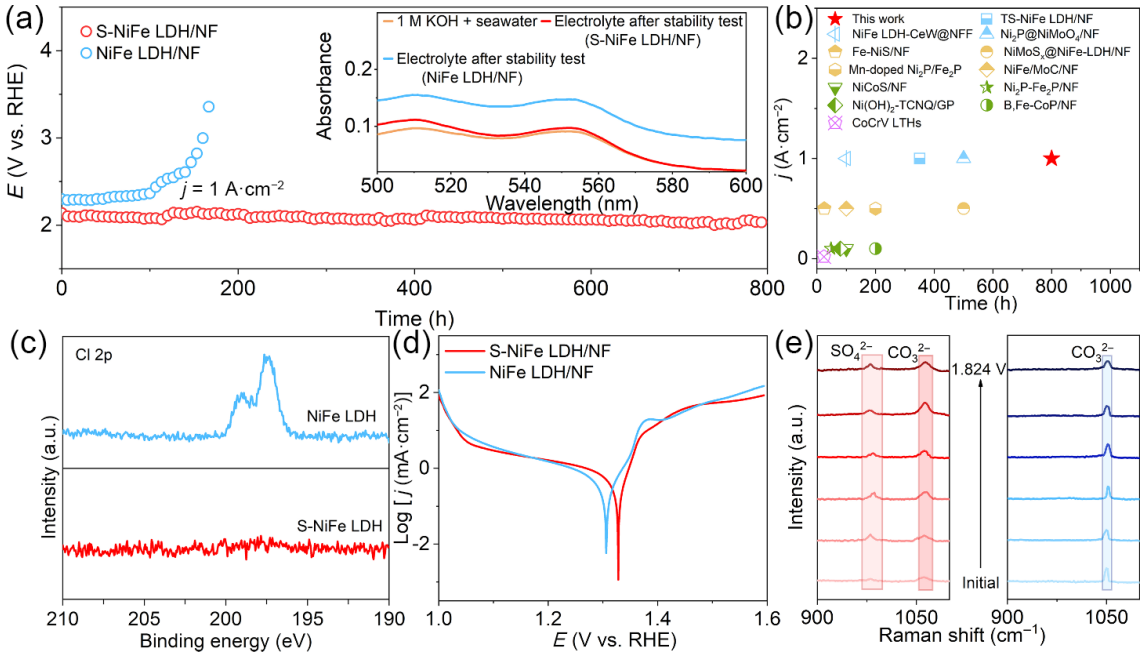

Figure 3 (a) Chronopotentiometric curves of S-NiFe LDH/NF and NiFe LDH/NF, with the inset showing the corresponding UV-vis absorption spectra of the electrolytes collected after stability testing at 1 A·cm^{-2}. (b) Comparison of electrolysis lifetime in 1 M KOH + seawater. (c) Cl 2p core-level signals of as-prepared two NiFe LDH-based samples recorded after the stability test. (d) Comparison of corrosion behaviors for as-prepared two NiFe LDH-based samples in alkaline seawater environment. (e) *In situ* Raman monitoring of the structural evolution for as-prepared two NiFe LDH-based samples during the ASO process.

diethyl-p-phenylenediamine (DPD) colorimetric technique [55]. The UV-vis spectra reveal that S-NiFe LDH/NF generated only trace amounts of reactive chlorine species. On the contrary, a significantly higher hypochlorite concentration was generated in the electrolyte when using the NiFe LDH/NF anode (Fig. 3(a) inset and Fig. S18 in the ESM), which can be further confirmed by the Cl 2p XPS analysis by post-stability test (Fig. 3(c)). As shown in Fig. S19 in the ESM, the experimentally measured amount of oxygen closely matches the theoretical calculations across the current range of 200–1000 mA·cm^{-2}. The combined evidence of low active chlorine content and high FE demonstrates pronounced selectivity of S-NiFe LDH/NF for the OER over the CER at high *j*. Electrochemical tests (Fig. 3(d) and Fig. S20 in the ESM) demonstrate that the catalyst possesses a more noble corrosion potential and a reduced corrosion current, all of which confirm its excellent corrosion resistance. The reaction mechanism was probed by *in situ* Raman spectroscopy (Fig. 3(e)). The spectrum for S-NiFe LDH/NF reveals the exclusive presence of a sulfate (SO_4^{2-}) species at 981 cm^{-1} alongside carbonate (CO_3^{2-}) at 1064 cm^{-1}, a fingerprint absent in the undoped NiFe LDH/NF catalyst which only shows carbonate [56, 57]. This indicates that *in-situ* formed SO_4^{2-} surface layer serves the dual role of a chloride-repelling barrier and a stabilizer for the active sites, which collectively underpin the significantly enhanced operational stability of the catalyst.

A two-electrode electrolyzer (S-NiFe LDH/NF||Pt/C/NF) was constructed to assess its practical applicability (Fig. 4(a)). As revealed in Fig. 4(b), the full electrolyzer required merely 1.90 V to achieve 100 mA·cm^{-2} in alkaline seawater, superior to industrial RuO_2/NF||Pt/C/NF (2.0 V). More significantly, the system exhibits a higher durability than other self-supported catalysts, demonstrated by its extraordinary durability reaching to 1000 h at 500 mA·cm^{-2} (Figs. 4(c) and 4(d), and Table S5 in the ESM). To better simulate industrial operating conditions, we demonstrated the stability of the two-electrode system at 60 °C. It maintained stable operation for 140 h at a *j* of 500 mA·cm^{-2}, which strongly confirms its potential for practical application (Fig. S21 in the ESM). Notably, the assembled full electrolyzer maintains high performance with only minor decay in various Cl^--containing electrolytes, highlighting its exceptional adaptability to different water sources (Fig. S22 in the ESM).

3 Conclusions

In summary, hydrothermal sulfur doping is proven as a viable strategy to greatly improve the anti-chlorine corrosion capacity of NiFe LDH anode in alkaline seawater electrolysis. Such S-NiFe LDH/NF delivers a *j* of 1000 mA·cm^{-2}, requiring a low η of only 345 mV while maintaining its OER activity for 800 h. The exceptional performance can be arisen from the *in-situ* generation of a protective SO_4^{2-} layer on the catalyst surface during ASO, which availably suppresses the CER, significantly boosting the corrosion resistance. Additionally, two-electrode system equipped with S-NiFe LDH/NF and Pt/C/NF demonstrated excellent durability by sustaining stable operation reaching to 1000 h in alkaline seawater. Our study affords a plentiful catalyst to enable durable oxygen evolution from alkaline seawater, while paving the way for designing chloride-resistant LDH-based anodes via hydrothermal sulfur doping, advancing the prospects of industrial seawater electrolysis.

Acknowledgements

I.S. is thankful to the Deanship of Scientific Research, Islamic University of Madinah, for support via post publishing program no-4.

Electronic Supplementary Material: Supplementary material (SEM images; XPS and UV-vis spectra; LSV, CV, FTacV, and chronopotentiometric curves; Tafel, TOF, and Nyquist plots; Tables S1–S3) is available in the online version of this article at https://doi.org/10.26599/NRE.2025.9120211.

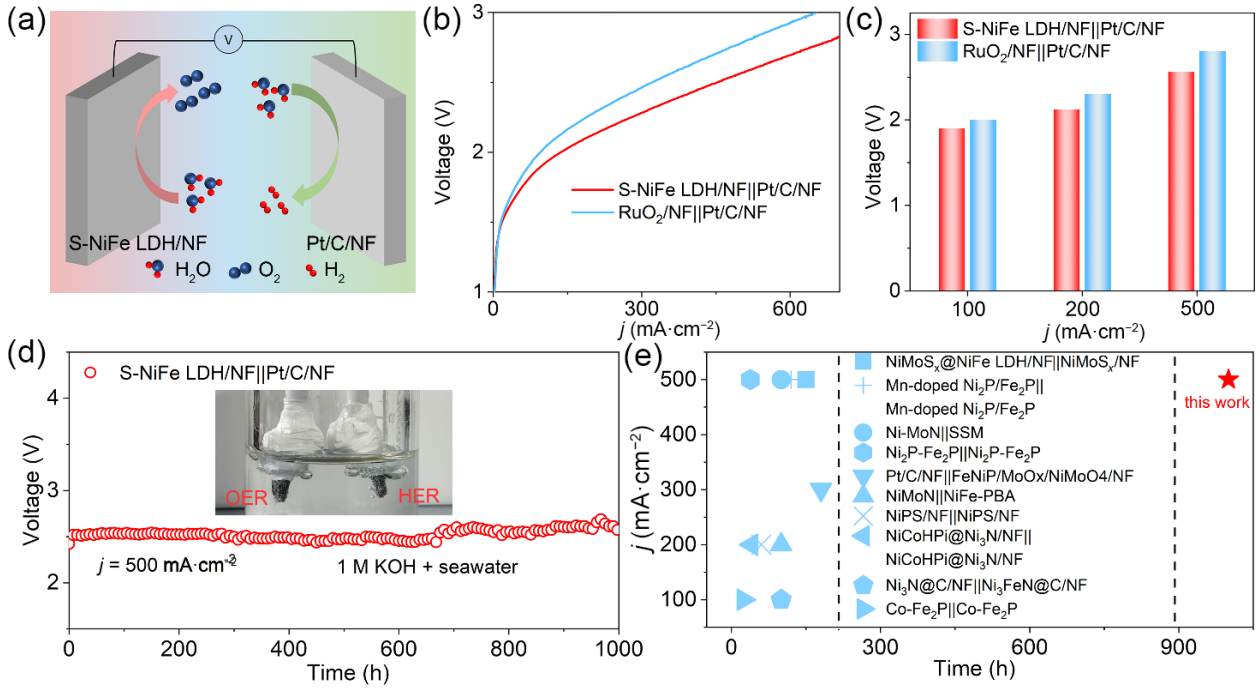

Figure 4 (a) Schematic of the experimental two-electrode cell assembly. Electrocatalytic performance in M KOH + seawater. (b) Polarization curves and (c) a comparative analysis of the operating voltages for S-NiFe LDH and the RuO_2-based full electrolyzer. (d) Operational stability of S-NiFe LDH-based full electrolyzer at j = 500 mA·cm^{-2} in 1 M KOH + seawater. (e) Comparison of electrolysis lifetime in 1 M KOH + seawater.

Declaration of conflicting interests

The authors declare no conflicting interests regarding the content of this article. Prof. Xuping Sun is an Associate Editor of *Nano Research Energy*.

Data availability

All data needed to support the conclusions in the paper are presented in the manuscript and/or the Supplementary Materials. Additional data related to this paper may be requested from the corresponding author upon request.

References

[1] Goel, M.; Sen, G. *Climate Action and Hydrogen Economy: Technologies Shaping the Energy Transition*; Springer: Singapore, 2024.

[2] Jiang, Z.; Ainiwaer, M.; Liu, J.; Ying, B. W.; Luo, F. M.; Sun, X. P. Hydrogen therapy: Recent advances and emerging materials. *Biomater. Sci.* **2024**, *12*, 4136–4154.

[3] Slezák, J.; Kura, B. *Molecular Hydrogen in Health and Disease*; Springer: Cham, 2024.

[4] Wang, J. H.; Cui, W.; Liu, Q.; Xing, Z. C.; Asiri, A. M.; Sun, X. P. Recent progress in cobalt-based heterogeneous catalysts for electrochemical water splitting. *Adv. Mater.* **2016**, *28*, 215–230.

[5] Cao, X. D.; Lin, B. L. Ultralow noble-metal-loaded senary high entropy alloy enables industrial-level alkaline hydrogen evolution. *Nano Res. Energy*, in press, DOI: 10.26599/NRE.2025.9120178.

[6] Haq, T.; Haik, Y. *Electrochemical Water Splitting: Fundamentals, Challenges and Advances*; Springer: Singapore, 2024.

[7] Postel, S. L. Entering an era of water scarcity: The challenges ahead. *Ecol. Appl.* **2000**, *10*, 941–948.

[8] Greve, P.; Kahil, T.; Mochizuki, J.; Schinko, T.; Satoh, Y.; Burek, P.; Fischer, G.; Tramberend, S.; Burtscher, R.; Langan, S. et al. Global assessment of water challenges under uncertainty in water scarcity projections. *Nat. Sustain.* **2018**, *1*, 486–494.

[9] Liang, J.; Cai, Z. W.; Li, Z. X.; Yao, Y. C.; Luo, Y. S.; Sun, S. J.; Zheng, D. D.; Liu, Q.; Sun, X. P.; Tang, B. Efficient bubble/precipitate traffic enables stable seawater reduction electrocatalysis at industrial-level current densities. *Nat. Commun.* **2024**, *15*, 2950.

[10] Sha, Q. H.; Wang, S. Y.; Yan, L.; Feng, Y. S.; Zhang, Z.; Li, S. H.; Guo, X. L.; Li, T. S.; Li, H.; Zhuang, Z. B. et al. 10,000-h-stable intermittent alkaline seawater electrolysis. *Nature* **2025**, *639*, 360–367.

[11] Sun, S. J.; Wang, K.; Li, X. X.; Li, Z. X.; Yang, C. X.; Chen, S. Y.; Shakir, I.; Sun, X. P.; Tang, B. Tailoring acidic microenvironment for enhanced electrocatalytic hydrogen generation from alkaline seawater. *Nano Res. Energy* **2025**, *4*, e9120199.

[12] Liang, J.; Li, Z. X.; Zhang, M.; Wang, H. F.; Cai, Z. W.; Luo, Y. S.; Luo, F. M.; Wu, T. W.; Yao, Y. C.; Tang, B. et al. Amorphous phosphates tailor local proton supply for alkaline hydrogen evolution electrocatalysis. *Adv. Mater.* **2025**, *37*, 2503660.

[13] Zhao, Y. Q.; Jin, B.; Zheng, Y.; Jin, H. Y.; Jiao, Y.; Qiao, S. Z. Charge state manipulation of cobalt selenide catalyst for overall seawater electrolysis. *Adv. Energy Mater.* **2018**, *8*, 1801926.

[14] Liang, J.; Li, Z. X.; He, X.; Luo, Y. S.; Zheng, D. D.; Wang, Y.; Li, T. S.; Ying, B. W.; Sun, S. J.; Cai, Z. W. et al. Electrocatalytic seawater splitting: Nice designs, advanced strategies, challenges and perspectives. *Mater. Today* **2023**, *69*, 193–235.

[15] Guo, J. X.; Zheng, Y.; Hu, Z. P.; Zheng, C. Y.; Mao, J.; Du, K.; Jaroniec, M.; Qiao, S. Z.; Ling, T. Direct seawater electrolysis by adjusting the local reaction environment of a catalyst. *Nat. Energy* **2023**, *8*, 264–272.

[16] Ren, Y. C.; Guo, Y. X.; Li, Z. X.; Hong, S. H.; Sun, S. J.; Yang, C. X.; Ibrahim, F, A.; Hamdy, M. S.; Gong, F.; Lv, Y. Q. et al. Palladium-chloride ion coordination stabilizes NiFe layered double hydroxides for alkaline seawater oxidation at industrial current densities. *J. Colloid Interface Sci.* **2025**, *700*, 138388.

[17] Ye, L.; Chen, Z. P.; Xu, X. Y.; Ma, F.; Fan, K. C.; Zong, L. B.; Wang, L.; Chen, G. J.; Li, X. W.; Zhan, T. R. Ultrafast room-temperature synthesis of phosphate-intercalated NiFe layered double hydroxides for high-performance alkaline seawater oxidation. *Inorg. Chem.* **2024**, *63*, 20859–20869.

[18] He, X.; Yao, Y. C.; Zhang, M.; Zhou, Y. L.; Zhang, L. M.; Ren, Y. C.; Dong, K.; Tang, H.; Nan, J.; Zhou, X. L. et al. Engineered PW_{12}-

polyoxometalate docked Fe sites on CoFe hydroxide anode for durable seawater electrolysis. *Nat. Commun.* **2025**, *16*, 5541.
[19] Wang, Z. K.; Wang, C.; Ye, L.; Liu, X. E.; Xin, L. T.; Yang, Y. Y.; Wang, L.; Hou, W. G.; Wen, Y. H.; Zhan, T. R. MnO_x film-coated NiFe-LDH nanosheets on Ni foam as selective oxygen evolution electrocatalysts for alkaline seawater oxidation. *Inorg. Chem.* **2022**, *61*, 15256–15265.
[20] Cai, Z. W.; Liang, J.; Li, Z. X.; Yan, T. Y.; Yang, C. X.; Sun, S. J.; Yue, M.; Liu, X. W.; Xie, T.; Wang, Y. et al. Stabilizing NiFe sites by high-dispersity of nanosized and anionic Cr species toward durable seawater oxidation. *Nat. Commun.* **2024**, *15*, 6624.
[21] Fan, R. L.; Liu, C. H.; Li, Z. H.; Huang, H. T.; Feng, J. Y.; Li, Z. S.; Zou, Z. G. Ultrastable electrocatalytic seawater splitting at ampere-level current density. *Nat. Sustain.* **2024**, *7*, 158–167.
[22] Yu, Y.; Ning, M. H.; Wang, Y.; Yuan, C. Q.; Ren, Z. F. Direct seawater electrolysis for hydrogen production. *Nat. Rev. Mater.* **2025**, *10*, 857–873.
[23] Liu, J. Y.; Duan, S.; Shi, H.; Wang, T. Y.; Yang, X. X.; Huang, Y. H.; Wu, G.; Li, Q. Rationally designing efficient electrocatalysts for direct seawater splitting: Challenges, achievements, and promises. *Angew. Chem., Int. Ed.* **2022**, *61*, e202210753.
[24] Gu, Y. H.; Zhang, Y. X.; Song, X. Y.; Wang, Y. N.; Bao, A.; Zhang, D. S.; Lv, J. Y.; Zheng, Z.; Zhang, X. Y.; Liu, Z. L. et al. Fluorine-induced surface protection strategy for bifunctional high entropy electrocatalysts enables stable seawater splitting. *Nano Res. Energy* **2025**, *4*, e9120189
[25] Zhang, Q.; Wang, Z. W.; Wang, L. H.; Wei, Z. C.; Zhuo, L. C.; Liu, Y. F.; Shakir, I.; Hu, G. Z.; Liu, X. J. Nano-hollow carbon-supported high-entropy alloy catalysts for energy-saving seawater electrolysis. *Nano Res. Energy* **2025**, *4*, e9120196.
[26] Li, H. W.; Zhang, L.; Liu, W. J.; Gui, T. Y.; Xiao, L. F.; Liu, Q.; Ding, J. Y.; Hu, G. Z.; Liu, X. J. Partial sulfidation engineering of a $Ni(OH)_2/NiS_x$ heterostructure towards sulfion oxidation-assisted seawater splitting. *Mater. Chem. Front.* **2025**, *9*, 2658–2667.
[27] Yang, M. S.; Ding, J. Y.; Wang, Z. W.; Zhang, J. W.; Peng, Z. M.; Liu, X. J. NiMo-based alloy and its sulfides for energy-saving hydrogen production via sulfion oxidation assisted alkaline seawater splitting. *Chin. Chem. Lett.* **2025**, *36*, 110861.
[28] Xu, J.; Kao, C. C.; Shen, H. F.; Liu, H.; Zheng, Y.; Qiao, S. Z. $Ru_{0.1}Mn_{0.9}O_x$ electrocatalyst for durable oxygen evolution in acid seawater. *Angew. Chem., Int. Ed.* **2024**, *64*, e202420615.
[29] Dionigi, F.; Reier, T.; Pawolek, Z.; Gliech, M.; Strasser, P. Design criteria, operating conditions, and nickel-iron hydroxide catalyst materials for selective seawater electrolysis. *ChemSusChem* **2016**, *9*, 962–972.
[30] Wang, Y. Y.; Yan, D. F.; El Hankari, S.; Zou, Y. Q.; Wang, S. Y. Recent progress on layered double hydroxides and their derivatives for electrocatalytic water splitting. *Adv. Sci.* **2018**, *5*, 1800064.
[31] Lv, L.; Yang, Z. X.; Chen, K.; Wang, C. D.; Xiong, Y. J. 2D layered double hydroxides for oxygen evolution reaction: From fundamental design to application. *Adv. Energy Mater.* **2019**, *9*, 1803358.
[32] Zhou, D. J.; Li, P. S.; Lin, X.; McKinley, A.; Kuang, Y.; Liu, W.; Lin, W. F.; Sun, X. M.; Duan, X. Layered double hydroxide-based electrocatalysts for the oxygen evolution reaction: Identification and tailoring of active sites, and superaerophobic nanoarray electrode assembly. *Chem. Soc. Rev.* **2021**, *50*, 8790–8817.
[33] Sahoo, D. P.; Das, K. K.; Mansingh, S.; Sultana, S.; Parida, K. Recent progress in first row transition metal layered double hydroxide (LDH) based electrocatalysts towards water splitting: A review with insights on synthesis. *Coord. Chem. Rev.* **2022**, *469*, 214666.
[34] Liu, H.; Shen, W.; Jin, H. Y.; Xu, J.; Xi, P. X.; Dong, J. C.; Zheng, Y.; Qiao, S. Z. High-performance alkaline seawater electrolysis with anomalous chloride promoted oxygen evolution reaction. *Angew. Chem., Int. Ed.* **2023**, *62*, e202311674.
[35] Zhang, L. C.; Liang, J.; Yue, L. C.; Dong, K.; Li, J.; Zhao, D. L.; Li, Z. R.; Sun, S. J.; Luo, Y. S.; Liu, Q. et al. Benzoate anions-intercalated NiFe-layered double hydroxide nanosheet array with enhanced stability for electrochemical seawater oxidation. *Nano Res. Energy* **2022**, *1*, 9120028.
[36] Song, J. Y.; Li, Z. X.; Sun, S. J.; Yang, C. X.; Cai, Z. W.; Wang, X. Y.; Yue, M.; Zhang, M.; Wang, H. F.; Farouk, A. et al. Citrate ions-modified NiFe layered double hydroxide for durable alkaline seawater oxidation. *J. Colloid Interface Sci.* **2025**, *679*, 1–8.
[37] Liang, J.; Cai, Z. W.; Li, Z. X.; Geng, M. Q.; Wang, H. F.; Wang, Z. Q.; Li, T. S.; Wu, T. W.; Luo, F. M.; Sun, X. P. et al. Expanded negative electrostatic network-assisted seawater oxidation and high-salinity seawater reutilization. *ACS Nano* **2025**, *19*, 1530–1546.
[38] Kuang, Y.; Kenney, M. J.; Meng, Y. T.; Hung, W. H.; Liu, Y. J.; Huang, J. E.; Prasanna, R.; Li, P. S.; Li, Y. P.; Wang, L. et al. Solar-driven, highly sustained splitting of seawater into hydrogen and oxygen fuels. *Proc. Natl. Acad. Sci. USA* **2019**, *116*, 6624–6629.
[39] Chen, H. C.; Liu, P. Y.; Li, W. B.; Xu, W. W.; Wen, Y.; J. Zhang, S. X.; Yi, L.; Dai, Y. Q.; Chen, X.; Dai, S. et al. Stable seawater electrolysis over 10,000 H via chemical fixation of sulfate on NiFeBa-LDH. *Adv. Mater.* **2024**, *36*, 2411302.
[40] Ren, Y. C.; Zhang, X. X.; Yang, C. X.; Li, Z. X.; Luo, Y. H.; Sun, S. J.; Ibrahim, F. A.; Hamdy, M. S.; Shakir, I.; Cui, G. W. et al. Durable ampere-scale seawater electrolysis driven by Ba-doped NiFe layered double hydroxide. *Inorg. Chem.* **2025**, *64*, 21185–21193.
[41] Dai, Q. Y.; Cai, Z. W.; Yang, C. X.; Li, Z. X.; Sun, S. J.; Yue, M.; Tang, X. L.; He, X.; Yuan, Y. J.; Tang, H. et al. Hexafluoroantimonate-intercalated NiFe layered double hydroxide enables stable alkaline seawater oxidation at ampere-level current densities. *Inorg. Chem. Front.* **2025**, *12*, 6132–6138.
[42] He, X.; Yao, Y. C.; Zhang, L. M.; Wang, H. F.; Tang, H.; Jiang, W. L.; Ren, Y. C.; Nan, J.; Luo, Y. S.; Wu, T. W. et al. Hexafluorophosphate additive enables durable seawater oxidation at ampere-level current density. *Nat. Commun.* **2025**, *16*, 4998.
[43] Ma, R. Z.; Sasaki, T. Nanosheets of oxides and hydroxides: Ultimate 2D charge-bearing functional crystallites. *Adv. Mater.* **2010**, *22*, 5082–5104.
[44] Wang, Q.; O'Hare, D. Recent advances in the synthesis and application of layered double hydroxide (LDH) nanosheets. *Chem. Rev.* **2012**, *112*, 4124–4155.
[45] Sun, X. G.; Shen, W.; Liu, H.; Xi, P. X.; Jaroniec, M.; Zheng, Y.; Qiao, S. Z. Corrosion-resistant NiFe anode towards kilowatt-scale alkaline seawater electrolysis. *Nat. Commun.* **2024**, *15*, 10351.
[46] Yang, C. X.; Bi, L. Y.; Cai, Z. W.; Li, Z. X.; Sun, S. J.; Wang, X. Y.; Zhang, M.; Yue, M.; Zheng, D. D.; Luo, Y. S. et al. Poly(3-thiophenemalonic acid) modified NiFe layered double hydroxide electrocatalyst for stable seawater oxidation at an ampere-scale current density. *ACS Mater. Lett.* **2024**, *6*, 5248–5255.
[47] Tyndall, D.; Craig, M. J.; Gannon, L.; McGuinness, C.; McEvoy, N.; Roy, A.; García-Melchor, M.; Browne, M. P.; Nicolosi, V. Demonstrating the source of inherent instability in NiFe LDH-based OER electrocatalysts. *J. Mater. Chem. A* **2023**, *11*, 4067–4077.
[48] Yuan, Y. J.; Wu, T.; Zhang, X. Y.; Wei, Z. H.; Tang, H. Iron foam-derived nickel-iron hydroxide nanosheets via solution etching as robust catalysts for alkaline seawater oxidation. *Chem. Commun.* **2025**, *61*, 15874–15877.
[49] Wu, J.; Huang, A.Q.; Hu, H.; Gao, X. H.; Chen, Z. W. Construction and enhancement of built-in electric field for efficient oxygen evolution reaction. *J. Colloid Interface Sci.* **2024**, *674*, 677–685.
[50] Liu, Y. J.; Hong, X. L.; Liu, X. Y.; Chen, W. J.; Tang, J. Electrolysis of seawater: An effective path to sustainable hydrogen production with sulfur-doped NiFe LDH/MXene@NF electrodes. *ACS Sustain. Chem. Eng.* **2024**, *12*, 11520–11530.
[51] Lei, H.; Ma, L.; Wan, Q. X.; Tan, S. Z.; Yang, B.; Wang, Z. L.; Mai, W. J.; Fan, H. J. Promoting surface reconstruction of NiFe layered double hydroxide for enhanced oxygen evolution. *Adv. Energy Mater.* **2022**, *12*, 2202522.
[52] Li, Q.; Luo, W. S.; Cui, X. Z.; Shi, J. L. Rapid and *in situ* active sites regeneration for OER activity recovery and greatly prolonged water-splitting performance. *Angew. Chem., Int. Ed.* **2025**, *64*, e202500303.

[53] Yang, C. X.; Guo, Y. X.; Sun, S. J.; Li, Z. X.; Yao, L.; Wang, H. F.; Zhang, M.; Yue, M.; Zheng, D. D.; Yao, Y. C. et al. PEDOT:PSS-modified NiFe layered double hydroxide enables efficient and durable seawater electrolysis at high current density. *J. Mater. Chem. A* **2025**, *13*, 25329–25334.
[54] Zhu, Y. M.; Wang, J. A.; Weiser, G.; Klingenhof, M.; Koketsu, T.; Liu, S. H.; Pi, Y. C.; Henkelman, G.; Shi, X.Y.; Li, J. Y. et al. Ru single atoms and sulfur anions dual-doped NiFe layered double hydroxides for high-current-density alkaline oxygen evolution reaction. *Adv. Energy Mater.* **2025**, *15*, 2500554.
[55] Vos, J.; Koper, M. T. M. Measurement of competition between oxygen evolution and chlorine evolution using rotating ring-disk electrode voltammetry. *J. Electroanal. Chem.* **2018**, *819*, 260–268.
[56] Chen, X. J.; Xu, K. Q.; Li, J. H.; Wang, X.; Zhao, T. T.; Liu, F. M.; Yu, M.; Cheng, F. Y. Ni_3S_2@$NiFeP_x$ electrode with dual-anion-modulated layer for efficient and stable oxygen evolution. *Chin. Chem. Lett.* **2023**, *34*, 108713.
[57] Deng, P. J.; Liu, Y.; Liu, H. L.; Li, X. N.; Lu, J. J.; Jing, S. Y.; Tsiakaras, P. Layered double hydroxides with carbonate intercalation as ultra-stable anodes for seawater splitting at ampere-level current density. *Adv. Energy Mater.* **2024**, *14*, 2400053.

Xuping Sun received his PhD degree in Changchun Institute of Applied Chemistry (CIAC), Chinese Academy of Sciences in 2006. During 2006–2009, he carried out postdoctoral researches at Konstanz University, University of Toronto, and Purdue University. In 2010, he started his independent research career as a Professor at CIAC and then moved to Sichuan University in 2015. During 2018–2024, he joined University of Electronic Science and Technology of China where he founded the Research Center of Nanocatalyst & Sensing. He is currently a professor at West China Hospital of Sichuan University and Shandong Normal University. He was recognized as a highly cited researcher (2018–2020) in both areas of chemistry and materials science by Clarivate Analytics. He published over 800 papers with total citations about 90000 and an h-index of 155.